Towards a Design Framework for High Pressure Turboexpanders

Joshua Kelly*, Sebastiano Fichera† and Sebastian Timme‡
School of Engineering, University of Liverpool, Liverpool, L69 3GH, United Kingdom

A design framework for the development of high pressure turboexpanders for use in waste energy recovery in natural gas extraction is proposed herein. An empirical model, implemented as part of this work, is used to rapidly calculate initial key geometric design parameters and to predict radial-inflow turbine performance characteristics, which are then compared to computational fluid dynamics predictions for an auxiliary power unit validation test case to successfully demonstrate the empirical model's accuracy. Preliminary steps in the optimisation procedure using the same computational fluid dynamics tool enabled with adjoint based gradient computation are discussed. It is shown that the set-up results in accurate gradient information of a chosen cost function with respect to the design parameters when compared with finite differencing. Necessary modifications to the treatment of wall boundaries and mesh deformation within the optimisation loop are outlined. Finally, an overview of the entire framework is presented.

I. Introduction

CLEAN and accessible energy, and related to this the ambition of the net-zero economy, is one of the defining challenges of our time facing modern engineering. Within the future energy mix, hydrogen takes a key role; both green and blue hydrogen are crucial for industrial decarbonisation with an ambition of 5 GW low carbon hydrogen production in the UK by 2030[1]. Most hydrogen research focuses on the cleanest green hydrogen, where hydrogen is produced by electrolysis using power generated from renewable energy sources. Blue hydrogen is produced when natural gas is split into hydrogen and carbon dioxide (CO_2), using either steam methane reforming or auto thermal reforming[3], and capturing and storing the residual CO_2. Similarly, grey hydrogen is produced without the capture of CO_2. This work sits in the context of the technological developments needed to produce blue hydrogen (and eliminate the need for grey hydrogen), with the potential of removing the high-powered diesel generators at source that produce significant harmful emissions[4]. Specifically, we look at the aerodynamic design optimisation of high-pressure turboexpanders.

Turboexpanders can be used for waste heat energy recovery in natural gas extraction operating in high pressure and high temperature (HPHT) wells. Such wells have significant potential energy that is currently unutilised; natural gas is currently extracted at 400 bar (and more) and expanded for processing. Turboexpanders can be used to recover energy during gas expansion that can be deployed to power the sequestration process during blue hydrogen production, with the aim of making this process net-zero at the source. Current commercial turboexpanders are limited to a maximum inlet pressure rating of approximately 200 bar[5]. It can be expected that increasing the inlet pressure can significantly increase the generated power output. Thus, the goal is to design a turboexpander that operates close to a natural gas well. For this goal to be achieved, there is a need to understand the complex fluid flow within an HPHT turboexpander.

To study the complex fluid flow through such HPHT turboexpanders in detail, a suitable geometry needs to be created first. This work proposes a framework to design geometries of turboexpanders via the application of preliminary empirical design and subsequent geometry optimisation using industry-standard computational fluid dynamics (CFD) methods enabled with adjoint gradient computation. Such a framework aims to greatly decrease the effort required in the early design phase. Existing preliminary methods can be used to generate sub-optimal designs that can be enhanced using modern optimisation methods to generate improved geometries for machines operating in unconventional/extreme conditions. The adjoint methodology is the state-of-the-art of gradient-based optimisation techniques. The implementation of optimisation methods in turbomachinery design is becoming increasingly prevalent as a method to improve the overall efficiency. These methods offer design solutions where there is a lack of experimental data or design guidelines. Combined this removes the need for an overly expensive

* PhD Student, J.Kelly7@liverpool.ac.uk
† Lecturer, sebastiano.fichera@liverpool.ac.uk
‡ Senior Lecturer, sebastian.timme@liverpool.ac.uk

early design process. Subsequently, highest-fidelity CFD methods can then be used to investigate the fluid phenomena present, which can help informed decision making in the design of a commercial turboexpander.

The adjoint method is a highly efficient way to evaluate optimal values of an objective function of an optimisation problem with an arbitrary number of design variables[6,7]. Significant advances have been achieved over the last four decades concerning its development and implementation into modern CFD packages. The method was first pioneered for external aerodynamics problem[8–10] but until recently has had limited application for turbomachinery problems due to the difficulty in deriving the internal boundary conditions. Early studies involved the optimisation of two-dimensional blade geometries[11,12] before being expanded to study isolated three-dimensional blades[13]. More recently multi-row optimisation has been performed after derivation of flow-consistent adjoint boundary conditions, a discrete mixing plane formulation and an automatic mesh deformation[14]. The designs produced by concurrent optimisations are generally better than optimisations performed in isolation. Eventually, using the adjoint method, any given optimisation problem will converge to an optimum. This work uses the adjoint method implemented in SU2, a C++ and Python collection of software tools for the analysis of partial differential equations and constrained optimisation problems.

The paper continues with an overview of an empirical approach for early-stage design in Section II. The overall CFD framework including the adjoint approach is summarised in Section III and the first results for the test case of an auxiliary power unit (APU) are presented in Section IV. Specifically, we demonstrate that empirical tools can produce good initial designs by estimating the key geometric dimensions of the APU test case, in addition to the performance characteristics when compared with a CFD simulation. Then we outline the optimisation procedure on the APU geometry to increase the machines efficiency. Validation of the adjoint based gradients with respect to finite-difference evaluation is presented. Required modifications in the optimisation loop itself are identified and discussed. Finally, the proposed framework for the design of such HPHT turboexpanders that implements adjoint optimisation method within the preliminary design phase is outlined.

II. Empirical Model

Preliminary design of turbomachinery takes up approximately 50% of the total project time[15] and success relies extensively on empirical methods and the designers' experience. Seminal work by Rohlik[16] and Glassman[17] developed empirical models for use in radial turbine design and provides the basis for the model used in this work. With this model, viscous losses are expressed in terms of a kinetic energy loss coefficient for both the stator and the rotor. The two-dimensional kinetic energy loss coefficient is given by

$$\bar{e}_{2D} = \frac{E\left(\frac{\theta_{\mathrm{tot}}}{l}\right)_{\mathrm{ref}}\left(\frac{Re}{Re_{\mathrm{ref}}}\right)^{-0.2}\left(\frac{l}{s}\right)}{\cos\Phi - \frac{t}{s} - H\left(\frac{\theta_{tot}}{l}\right)_{\mathrm{ref}}\left(\frac{Re}{Re_{\mathrm{ref}}}\right)^{-0.2}\left(\frac{l}{s}\right)}$$

where the flow angle Φ is given by α_1 for the stator definition and the β_2 for the rotor. Here, θ is the momentum thickness, l is the blade surface length from leading to trailing edge, Re is the Reynolds number, t is the trailing edge thickness and s is the blade spacing at blade-row exit. The subscript ref refers to a reference value taken from experimental measurements. The factors for energy E and form H are defined using a velocity profile exponent of 0.2, with further details on this described by Glassman[17,18]. The ratio between the two-dimensional loss coefficient and its three-dimensional counterpart is assumed to be equal to the ratio of the three-dimensional to two-dimensional surface areas, expressed as

$$\bar{e}_{3D} = \bar{e}_{2D}\left(\frac{A_{3D}}{A_{2D}}\right)$$

For details on the calculation of terms and the overall procedure, the reader is directed to the work by Glassman[17]. Five losses are considered in the empirical model; disk friction, tip clearance, exit velocity, and rotor and stator losses. Flow analysis is assumed one-dimensional at the stator inlet and outlet and the rotor inlet, but an axisymmetric two-dimensional analysis is performed at the rotor outlet where there is variation in the flow field along the outlet radius. The calculation routine, implemented as part of this work, can be briefly described in the following steps:

1. The model initialises a stator geometry based on user inputs and estimates the stator exit and stator inlet flow properties and calculates the stator loss coefficient. The inlet velocity and static flow properties are iteratively calculated until the respective values converge by comparing differences between subsequent iterations until a user-specified tolerance is achieved.
2. Next, the rotor inlet flow properties are determined using a rotor inlet flow angle defined by a user input. The windage loss is then calculated iteratively until convergence is achieved.

3. Two-dimensional axisymmetric analysis is performed at the rotor outlet to calculate the outlet flow properties for varying flow field radius. The corresponding rotor loss coefficient is then calculated and the exit velocities, flow angles and static flow properties are recomputed. Mass flow rate at the outflow is calculated and compared to the input mass flow value. If necessary, the kinematic outflow variables are recalculated according to modification determined by a parabolic curve fitting bisection algorithm until continuity is achieved. If the fluid energy requirement is not fulfilled by these modifications, this step is repeated until the requirement is satisfied.
4. Finally, the exit flow properties are finalised and the losses, efficiency reduction contributions and specific speed are calculated. For parametric studies, the code then repeats for varying user input.

III. Methodology

A. Governing Equations

The flow is assumed to be governing by the Reynolds-averaged Navier-Stokes (RANS) equations coupled with a suitable turbulence model. The k-ω shear-stress-transport (SST) model is used herein to close the turbulence problem. Internal turbomachinery flow problems require the solution of the compressible form of the governing equations given as

$$\frac{\partial \boldsymbol{U}}{\partial \mathrm{t}} + \nabla \cdot \boldsymbol{F}^c - \nabla \cdot \boldsymbol{F}^v = \boldsymbol{Q}$$

where the conservative variables are given by $\boldsymbol{U} = \{\rho, \rho\boldsymbol{u}, \rho E, \rho k, \rho\omega\}^T$ with ρ as density, $\rho\boldsymbol{u}$ as momentum, ρE as energy, ρk as turbulent kinetic energy and $\rho\omega$ as dissipation rate. The convective and viscous fluxes and the source term are given by

$$\boldsymbol{F}^c = \begin{Bmatrix} \rho\boldsymbol{u} \\ \rho\boldsymbol{u} \otimes \boldsymbol{u} + \bar{\bar{I}}p \\ \rho E\boldsymbol{u} + p\boldsymbol{u} \\ \rho k\boldsymbol{u} \\ \rho\omega\boldsymbol{u} \end{Bmatrix} \quad \boldsymbol{F}^v = \begin{Bmatrix} \cdot \\ \bar{\bar{\tau}} \\ \bar{\bar{\tau}} \cdot \boldsymbol{u} + \kappa_{\text{eff}}\nabla T \\ -(\mu_{dyn} + \sigma_k\mu_{tur})\nabla k \\ -(\mu_{dyn} + \sigma_k\mu_{tur})\nabla\omega \end{Bmatrix} \quad \boldsymbol{Q} = \begin{Bmatrix} q_\rho \\ \boldsymbol{q}_{\rho\boldsymbol{u}} \\ q_{\rho E} \\ P - \beta^*\rho\omega k \\ \frac{\gamma}{\nu_t}P - \beta^*\rho\omega^2 + 2(1-F_1)\frac{\rho\sigma_{\omega 2}}{\omega}\nabla k\nabla\omega \end{Bmatrix}$$

The viscous stress tensor expressed in vector notation for this case is given by

$$\bar{\bar{\tau}} = \mu_{\text{eff}}\left(\nabla\boldsymbol{u} + \nabla\boldsymbol{u}^T - \frac{2}{3}\bar{\bar{I}}(\nabla \cdot \boldsymbol{u})\right) - \frac{2}{3}\rho k\delta_{ij}$$

The effective dynamic viscosity μ_{eff} is calculated, following the Boussinesq assumption, as the sum of laminar and turbulent components, whereby the laminar part follows Sutherland's viscosity law and the turbulent part results from the turbulence modelling. Similar arguments apply to the coefficient of thermal conductivity κ_{eff}. For the turbulence model, the values for the remaining constants, blending functions and auxiliary relations follow the original model[19,20]. To ensure the accuracy of the flow solution in the optimisation procedure a validation simulation was performed. The results of this are presented in Section IV.B.

B. Spatial Discretization and Time Stepping

A vertex-based RANS solver is implemented in SU2. The RANS equations are discretized using a finite volume method[21] with a standard edge-based structure on a dual grid with control volumes that are constructed using a medial-dual based scheme[22]. This method allows the solver to use structured, unstructured and hybrid grids. The semi-discretised form of the governing equations is given by

$$\int_{\Omega_i}\frac{\partial \boldsymbol{U}}{\partial t}d\Omega + \sum_{j\in\mathcal{N}(i)}\left(\tilde{\boldsymbol{F}}_{ij}^c + \tilde{\boldsymbol{F}}_{ij}^v\right)\Delta S_{ij} - \boldsymbol{Q}|\Omega_i| = \int_{\Omega_i}\frac{\partial \boldsymbol{U}}{\partial t}d\Omega + \boldsymbol{R}_i(\boldsymbol{U}) = 0$$

where $\boldsymbol{R}_i(\boldsymbol{U})$ is the residual vector obtained via the integration of all the spatial terms over the control volume Ω_i. A first order Roe upwind method[23] is used to discretize the convective terms. The viscous terms are discretized using the average-gradient method and the spatial gradients of flow variables themselves are calculated using the Green-Gauss method.

The turbine blades, hub and shroud enforce a no-slip boundary condition. The inlet, outlet and interface between blade rows use non-reflecting boundaries with a total temperature and pressure condition at stator inflow and static pressure condition at diffuser outlet. More details about the implementation of the mixing-plane method are given in the Section III.C below.

Time stepping for steady state convergence uses an implicit backward Euler scheme with the resulting linear algebraic equation

$$\left(\frac{|\Omega|}{\Delta t^n}\delta_{ij} + \frac{\partial \boldsymbol{R}(\boldsymbol{U}^n)}{\partial \boldsymbol{U}^n}\right)\Delta \boldsymbol{U}^n = -\boldsymbol{R}(\boldsymbol{U}^n)$$

where the pseudo time-step Δt differs in each cell using a standard local time-stepping technique. For multiple fluid domains coupled with mixing-plane interfaces, the residuals along the boundary are also dependent on the solution of adjacent fluid domains. This dependency is treated explicitly meaning that the residuals at iteration step n in the fluid domain j depends on the solution of the adjacent fluid domain k computed at iteration step $(n-1)$. This results in a slight modification of the above equation as,

$$\left(\frac{|\Omega|}{\Delta t^n}\delta_{ij} + \frac{\partial \boldsymbol{R}(\boldsymbol{U}^n)}{\partial \boldsymbol{U}^n}\right)_{\mathrm{j}}\Delta \boldsymbol{U}_j^n = -\boldsymbol{R}(\boldsymbol{U}_j^n, \boldsymbol{U}_k^{n-1})$$

The resulting linear system for the solution update $\Delta \boldsymbol{U}_j^n$ is solved with the flexible generalized minimal residual method[24] with preconditioning using an incomplete lower-upper factorisation. Both the outlet pressure and rotational speed of the rotor are linearly increased from zero over the first 500 iterations to accelerate convergence. A Courant-Friedrichs-Lewy (CFL) number of 20 is used for the local time-step calculation. Using the implicit backward Euler formulation results in an approximate Newton method for solving $\boldsymbol{R}(\boldsymbol{U})$. If the solution is sufficiently converged, the resulting solution $\boldsymbol{U}$ only depends on the right-hand side of the linear system, therefore the left-hand side can be any reasonable approximation of the Jacobian operator $\partial \boldsymbol{R}/\partial \boldsymbol{U}$[25]. The solution process of the coupled equations, $\boldsymbol{R}(\boldsymbol{U}) = 0$, is transformed into a fixed-point iteration where the feasible flow and turbulent solutions can be calculated from the expression

$$\boldsymbol{U}^{n+1} = \boldsymbol{U}^n - P^{-1}(\boldsymbol{U}^n)\boldsymbol{R}(\boldsymbol{U}^n) =: \boldsymbol{G}(\boldsymbol{U}^n)$$

As there is a loose coupling between the flow and turbulent equations, the preconditioner P can be expressed as

$$P(\boldsymbol{U}) \coloneqq \begin{pmatrix} \frac{|\Omega|}{\Delta t^n}\delta_{ij} + \frac{\partial \widetilde{\boldsymbol{R}}_f(\boldsymbol{U}^n)}{\partial \boldsymbol{U}_f} & 0 \\ 0 & \frac{|\Omega|}{\Delta t^n}\delta_{ij} + \frac{\partial \widetilde{\boldsymbol{R}}_t(\boldsymbol{U}^n)}{\partial \boldsymbol{U}_t} \end{pmatrix} \approx \frac{\partial \boldsymbol{R}(\boldsymbol{U})}{\partial \boldsymbol{U}}$$

whereby the tilde indicates a suitable approximation to the exact partial Jacobian matrices and subscripts f and t indicate the equations of mean flow and turbulence model, respectively. It follows that G is stationary only at feasible points, therefore

$$\boldsymbol{R}(\boldsymbol{U}^*) = 0 \Leftrightarrow \boldsymbol{U}^* = \boldsymbol{G}(\boldsymbol{U}^*)$$

where $\boldsymbol{U}^*$ is the vector of conservative variables and $\boldsymbol{G}$ is the iteration operator of the pseudo time-stepper.

More details on the optimisation procedure, where the adjoint solution resulting from solving the previous equation are used, are given in Section III.D below.

C. Mixing Plane Method

Turbomachinery simulation requires a method to model the rotating components. When the flow between adjacent blades is non-uniform, it is necessary to implement a method to couple the two blade zones. The mixing plane method performs quasi-steady multistage turbomachinery calculations. Each fluid domain is modelled as a steady-state problem and a pitch-wise averaging process at the interface between stationary and rotating components provides the boundary conditions for downstream blade zones[26]. For this work the fluid zones are coupled via a non-reflecting interface[27]. For each node i along a spanwise band, ζ, of the interface, the characteristic jump consists of an average component and a harmonic component.

$$\delta \boldsymbol{c}_{i,\zeta} = \delta \bar{\boldsymbol{c}}_{\zeta} + \delta \boldsymbol{c}_{i,\zeta}$$

The average component $\delta \bar{\boldsymbol{c}}$ is the characteristic contribution that ensures the flow quantities match at the interface[28]. The average characteristic jump across the given spanwise band is calculated by

$$\begin{pmatrix} \delta\bar{c}_1 \\ \delta\bar{c}_2 \\ \delta\bar{c}_3 \\ \delta\bar{c}_4 \\ \delta\bar{c}_5 \end{pmatrix}_\zeta = \begin{bmatrix} -\bar{a}^2 & 0 & 0 & 0 & 1 \\ 0 & 0 & \bar{\rho}\bar{a} & 0 & 0 \\ 0 & 0 & 0 & \bar{\rho}\bar{a} & 0 \\ 0 & \bar{\rho}\bar{a} & 0 & 0 & 1 \\ 0 & -\bar{\rho}\bar{a} & 0 & 0 & 1 \end{bmatrix}_\zeta \begin{pmatrix} \rho^d - \bar{\rho}^t \\ v_n^d - \bar{v}_n^t \\ v_\theta^d - \bar{v}_\theta^t \\ v_\zeta^d - \bar{v}_\zeta^t \\ p^d - \bar{p}^t \end{pmatrix}_\zeta$$

with superscripts d and t referring to donor and target, respectively. Here $(\bar{\rho}, \bar{\boldsymbol{v}}, \bar{p})$ are averaged at each spanwise level. In cases where there is a different number of spanwise levels across the target and donor side a linear interpolation algorithm is used to determine the averaged flow quantities. This mixing plane method is conservative for mass, momentum and energy fluxes, if, and only if, the primitive variables are averaged using the mixed-out procedure[27].

The discrete form of the spatial Fourier transform of an outgoing characteristic c_j, modified for calculation on unstructured grids, is given by

$$\hat{c}_{j,k,\zeta} = \frac{1}{\theta_{\text{pitch}}} \sum_{i==}^{n_\zeta - 1} c_{j,i,\zeta} e^{-\left(\frac{2\pi i k}{\theta_{\text{pitch}}}\right)\theta_i} \Delta\theta_i\,, \qquad \text{with } \left(-\frac{n_\zeta}{2} + 1 < k < \frac{n_\zeta}{2} - 1\right)$$

This modification of the original work by Saxer and Giles[27] is derived in the work by Vitale et al.[28]. Each Fourier decomposition of the outgoing characteristics is then linearly combined and transformed into the spatial domain resulting in the harmonic component $\delta\dot{\boldsymbol{c}}_{i,\zeta}$. The two components are then converted into a primitive variable perturbation, which is used to determine the numerical convective flux.

D. Discrete Adjoint Optimisation

Following previous work[29], a generic optimisation problem can be represented as

$$\begin{aligned} &minimize && J(\boldsymbol{U}, \boldsymbol{D}, X) \\ &s.t. && \boldsymbol{U} = \boldsymbol{G}(\boldsymbol{U}, X) \\ & && X = M(\boldsymbol{D}) \end{aligned}$$

where the objective function J is a function of the flow variables $\boldsymbol{U}$, the design variables $\boldsymbol{D}$, and according to a surface deformation based on the current value of the design variables. A mesh deformation is performed using the linear elasticity method to create a new mesh X. The mesh deformation is formally handled in the constraint $X = M(\boldsymbol{D})$. Here $\boldsymbol{G}(\boldsymbol{U})$ is obtained from the result in Section IIIB. To evaluate the gradients of the objective function with respect to the design variables, first the Lagrangian is applied such that

$$\begin{aligned} \mathcal{L}(\boldsymbol{D}, \boldsymbol{U}, X, \bar{\boldsymbol{U}}, \bar{X}) &= J(\boldsymbol{U}, X) + [\boldsymbol{G}(\boldsymbol{U}, X) - \boldsymbol{U}]^T \bar{\boldsymbol{U}} + [M(\boldsymbol{D}) - X]^T \bar{X} \\ &= N(\boldsymbol{U}, \bar{\boldsymbol{U}}, X) - \boldsymbol{U}^T \bar{\boldsymbol{U}} + [M(\boldsymbol{D}) - X]^T \bar{X} \end{aligned}$$

where N is the shifted Lagrangian

$$N(\boldsymbol{U}, \bar{\boldsymbol{U}}, X) \coloneqq J(\boldsymbol{U}, X) + \boldsymbol{G}^T(\boldsymbol{U}, X)\bar{\boldsymbol{U}}$$

The resulting Lagrangian is then differentiated with respect to the design variables $\boldsymbol{D}$ using the chain rule. The adjoint variables $\bar{X}$ and $\bar{\boldsymbol{U}}$ are chosen to eliminate their dependency on the flow sensitivity $\partial\boldsymbol{U}/\partial\boldsymbol{D}$ and mesh sensitivity $\partial X/\partial\boldsymbol{D}$. This results in formulations for the adjoint variables as follows

$$\begin{aligned} \bar{\boldsymbol{U}} &= \frac{\partial}{\partial \boldsymbol{U}} N(\boldsymbol{U}, \bar{\boldsymbol{U}}, X) = \frac{\partial}{\partial \boldsymbol{U}} J^T(\boldsymbol{U}, X) + \frac{\partial}{\partial \boldsymbol{U}} \boldsymbol{G}^T(\boldsymbol{U}, X)\bar{\boldsymbol{U}} \\ \bar{X} &= \frac{\partial}{\partial X} N(\boldsymbol{U}, \bar{\boldsymbol{U}}, X) = \frac{\partial}{\partial X} J^T(\boldsymbol{U}, X) + \frac{\partial}{\partial X} \boldsymbol{G}^T(\boldsymbol{U}, X)\bar{\boldsymbol{U}} \end{aligned}$$

The resulting adjoint equations are fixed-point and can be solved in the same style as the flow solver detailed prior. Since $\boldsymbol{U} = \boldsymbol{G}(\boldsymbol{U}, X)$ for all values of $\boldsymbol{D}$, $\boldsymbol{\mathcal{L}} = J$ for all values of $\bar{\boldsymbol{U}}$, $\bar{X}$ and $\boldsymbol{D}$. Therefore, taking the derivative of the Lagrangian results in the total derivative of J, resulting in

$$\frac{dL}{d\boldsymbol{D}}^T = \frac{dJ}{d\boldsymbol{D}}^T = \frac{d}{d\boldsymbol{D}} M^T(\boldsymbol{D})\bar{X}$$

The adjoint equation does not depend on any design variable, so the gradient of a scalar objective function can be determined by solving only two sets of equations. A flow chart of this generic optimisation procedure implemented in SU2 is shown in Figure 1. For this work the discrete adjoint method is used. For multistage turbomachinery the set of equations for single flow domains must be modified for application to multiple flow domains coupled by a steady mixing plane interface. For an objective function or a constraint J of a multistage turbomachinery design

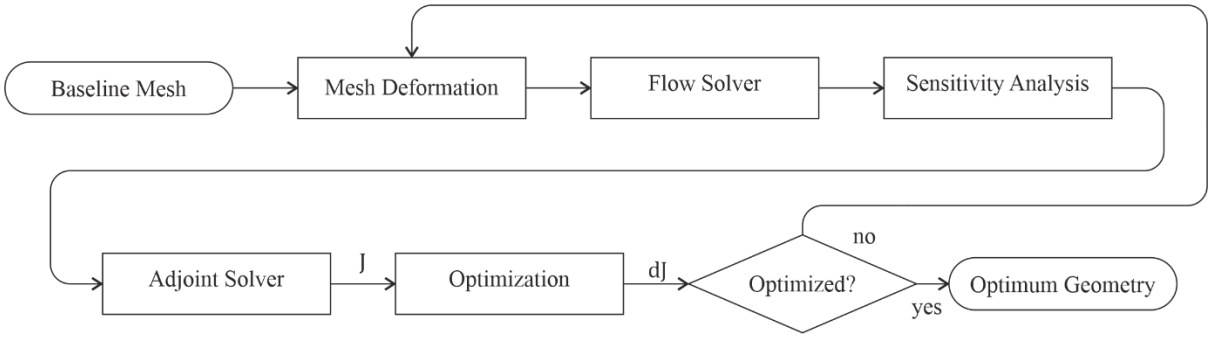

Figure 1 Flow chart of SU2 generic adjoint optimisation procedure

problem where the flow solution is obtained by solving the RANS equations on N flow domains; with the goal of this optimisation problem is to minimize the objective function. The mesh and the surface deformation are performed with linear elasticity equations and free-form deformation (FFD) algorithm.

The resulting optimisation problem can be expressed as

$$\begin{aligned} &minimize && J[\boldsymbol{U}_1(\boldsymbol{D}), \boldsymbol{X}_1(\boldsymbol{D}_1), \dots, \boldsymbol{U}_N(\boldsymbol{D}), \boldsymbol{X}_N(\boldsymbol{D}_N)] \\ &s.t. && \boldsymbol{U}_k = \boldsymbol{G}_k(\boldsymbol{U}, \boldsymbol{X}_k), \quad with\ k = 1, 2, \dots, N \\ & && \boldsymbol{X}_k = \boldsymbol{M}_k(\boldsymbol{D}_k), \quad with\ k = 1, 2, \dots, N \end{aligned}$$

with

$$\begin{aligned} \boldsymbol{D} &= \{\boldsymbol{D}_1, \boldsymbol{D}_2, \dots, \boldsymbol{D}_N\} \\ \boldsymbol{U} &= \{\boldsymbol{U}_1, \boldsymbol{U}_2, \dots, \boldsymbol{U}_N\} \end{aligned}$$

The resulting the Lagrangian can be expressed as

$$\begin{aligned} &\mathcal{L}(\boldsymbol{D}, \boldsymbol{U}, \boldsymbol{X}, \overline{\boldsymbol{U}}, \overline{\boldsymbol{X}}) \\ &= J(\boldsymbol{U}, \boldsymbol{X}) + [\boldsymbol{G}_1(\boldsymbol{U}, \boldsymbol{X}_1) - \boldsymbol{U}_1]^T + \cdots + [\boldsymbol{G}_N(\boldsymbol{U}, \boldsymbol{X}_N) - \boldsymbol{U}_N]^T \\ &\quad + [\boldsymbol{M}_1(\boldsymbol{D}_1) - \boldsymbol{X}_1]^T \overline{\boldsymbol{X}}_1 + \cdots + [\boldsymbol{M}_N(\boldsymbol{D}_N) - \boldsymbol{X}_N]^T \overline{\boldsymbol{X}}_N \end{aligned}$$

After differentiation of the above Lagrangian and appropriate selection of $\overline{\boldsymbol{X}}_k$ and $\overline{\boldsymbol{U}}_k$ such that dependency on the design variables can be eliminated, there remains N adjoint equations

$$\begin{aligned} &\overline{\boldsymbol{U}}_k = \frac{\partial}{\partial \boldsymbol{U}_k} J^T(\boldsymbol{U}, \boldsymbol{X}) + \sum_{i=1}^{N} \frac{\partial}{\partial \boldsymbol{U}_k} \boldsymbol{G}_i^T(\boldsymbol{U}, \boldsymbol{X}_i) \overline{\boldsymbol{U}}_i\,, \\ &with\ k = 1, 2, \dots, N \end{aligned}$$

and N mesh sensitivity equations

$$\begin{aligned} &\overline{\boldsymbol{X}}_k = \frac{\partial}{\partial \boldsymbol{U}_k} J^T(\boldsymbol{U}, \boldsymbol{X}) + \frac{\partial}{\partial \boldsymbol{X}_k} \boldsymbol{G}_k^T(\boldsymbol{U}, \boldsymbol{X}_k) \overline{\boldsymbol{U}}_i \\ &with\ k = 1, 2, \dots, N \end{aligned}$$

When all adjoint solutions $\overline{\boldsymbol{U}}_k$ are obtained, the mesh node sensitivity $\overline{\boldsymbol{X}}_k$ at each flow domain is computed and the N total derivatives of J with respect to the design variables of each kth domain is given by

$$\frac{dJ^T}{d\boldsymbol{D}_k} = \frac{d}{d\boldsymbol{D}_k} \boldsymbol{M}_k^T(\boldsymbol{D}_k) \overline{\boldsymbol{X}}_k, \qquad with\ k = 1, 2, \dots, N$$

The required derivatives are computed using the reverse mode of the open-source algorithmic differentiation tool CodiPack. The mesh surface deformation is performed using linear elasticity[30] according to the Free-Form Deformation procedure of Sederberg and Parry[31]. A flow chart of the generic procedure implemented in SU2 is shown in Figure 1.

Table 1: APU test case

$T_{tot,in}$	477.6 K
$p_{tot,in}$	413.6 kPa
β_{in}	0.0°
p_{out}	72.4 kPa
Ω	71700 rpm
$I_{turb,in}$	0.05
μ_{turb}/μ_{lam}	100.0

Table 2 Meridional channel and flow quantities comparison to empirical model

Meridional Channel Geometry			**Flow Quantities**		
Dimension	Present	Empirical	Property	CFD	Empirical
$R_{in,nozzle}$ **[mm]**	74	73.15	$p_{in,rotor}$ [Pa]	212072	215681
$R_{out,nozzle}$ **[mm]**	63.5	63.1	$M_{out,stator}$ [m/s]	0.922	0.961
$R_{in,rotor}$ **[mm]**	58.2	57.8	$\rho_{in,rotor}$ [kg/m^3]	1.820	1.864
$R_{out,rotor}^{tip}$ **[mm]**	36.8	36.6	$p_{out,rotor}$ [Pa]	66000	66206
h_{stator} **[mm]**	6.35	6.33	$M_{n,out,rotor}$ [m/s]	0.433	0.421
$h_{rotor,exit}$ **[mm]**	21.6	20.7	$\rho_{out,rotor}$ [kg/m^3]	0.7501	0.7732

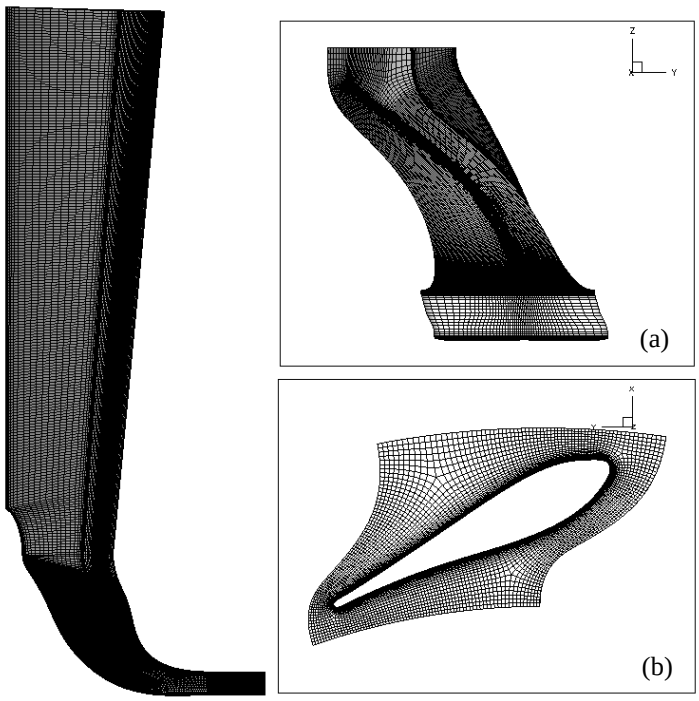

Figure 2 Blade geometry

IV. Results

A. Auxiliary Power Unit Test Case

The APU test case is a high-pressure ratio single-stage radial turbine test case based on the experimental campaign using the Sundstrand Power Systems T-100 Multipurpose Small Power Unit[32]. Full reconstruction of the turbine geometry for the purpose of academic validation was enabled by the work of Sauret[33 33] – and it is the most prevalent publicly available test case for radial machines. This test case has been used extensively in the literature as a validation case for preliminary design tools and CFD codes. Herein a design pressure ratio of 5.7

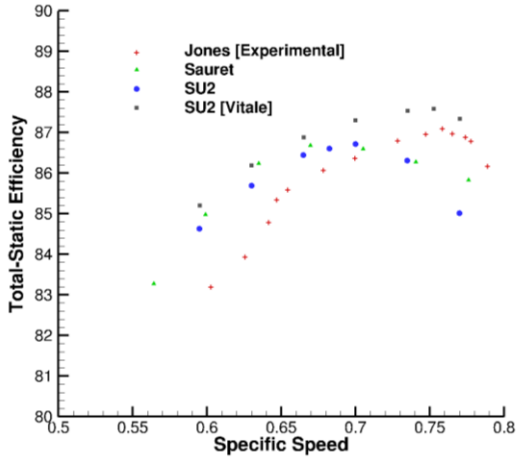

Figure 3 Comparison of numerical predictions and experimental data of total-to-static efficiency for the APU turbine at varying rotational speed

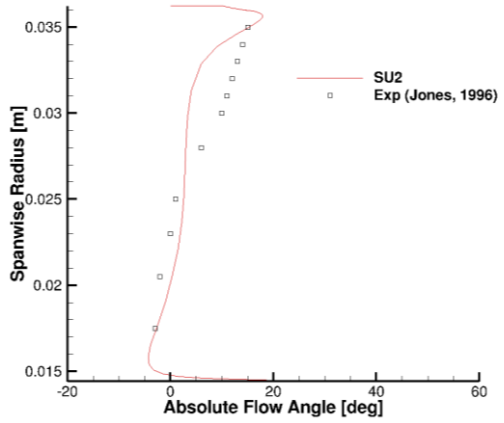

Figure 4 Comparison of absolute flow angle at the outlet for SU2 and experimental results

was use with the remaining relevant parameters shown in Table 1. A mesh was constructed based on the detailed geometry[14] using the open-source blade parametrisation tool Parablade[34] and the commercial automated turbomachinery meshing software ANSYS Turbogrid. Conformal meshing across the blade tip was ensured by using hybrid structured and unstructured mesh elements. Hexahedral elements were chosen from the leading edge of the rotor blade to enforce a conformal mapping until the interior angles become two large and the elements become too distorted, following which wedge elements were used. A normalised wall spacing of $y^+ \leq 1.0$ at the wall boundaries was enforced to ensure the viscous sub-layer of the flow is properly captured. The resulting grid contained 3.5 million elements. Insufficient information is provided in the literature regarding the shape of the spinner so a spherical shape was chosen as this facilitates convergence and prevents distorted mesh elements through the growth of the diffuser. Only one blade passage was meshed and was simulated using rotational periodic boundaries. An overview of the geometry is shown in Figure 2.

B. CFD Validation

A parametric study was performed to investigate the variation of total-to-static efficiency with varying specific speed and compare the flow solver predictions to experimental data and previous CFD studies. The rotational speed of the turbine was varied between 85% and 110% of its nominal value, which corresponds to a specific speed of $u/v_{ax} = 0.7$ where v_{ax} is the spouting velocity and u is the rotational speed of the rotor. The results shown in Figure 4 demonstrate good agreement between both experimental results and numerical studies conducted by other authors[28,33]. After discussion with the author[28], the significant variation between results obtained in this validation study and other work conducted using SU2 is expected to be due to a variation in the treatment of the mixing-plane between the rotor and the diffuser. The computational predictions match the trend of the experimental results; however, the peak efficiency is at the nominal design speed, but it still reduces with

both increasing and decreasing specific speed. There is a sharp decrease in efficiency when increasing the specific speed past the point of peak efficiency.

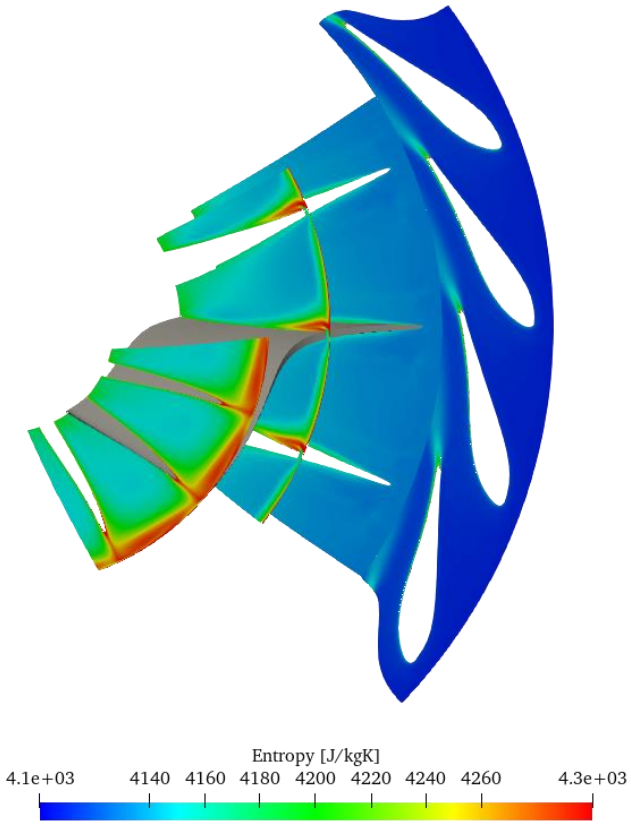

Figure 5 Entropy contour through APU turbine

The CFD predictions were subsequently compared to the empirical model to validate the empirical model's accuracy. Using an initial geometry with inputs taken from Jones[32] and Sauret[33], and the boundary conditions shown in Table 1, the calculated meridional channel geometry is compared to the present geometry and predicted flow quantities compared to the CFD results in Table 2. The empirical model predicts the meridional channel geometry well, with the largest variation between the present sizing and prediction is 1.1%. The flow quantities are also well predicted. The empirical model consistently gives higher density (>2.5% error) at blade zone boundaries than SU2, which is suspected to be due to the averaging process in the mixing plane present in the CFD results. The normal Mach number is presented at the outlet as the empirical model does not account for blade sweep so incorrectly predicts absolute velocities at the rotor outlet.

The performance characteristics are also well predicted. The empirical model results in a total-to-static efficiency of 86.4% at the nominal design point, a <1% difference to SU2. Additionally, the empirical tool can calculate the contributions to efficiency loss from five sources. The model predicts that 42% of the contribution to efficiency reduction will be generated through losses due to viscous losses in the rotor. A comparison between the absolute flow angle at the rotor outlet is presented in Figure 4. The trend of the flow angle is agreeable with the experimental results, while the location of the mixing-plane and the averaging process is suspected to cause the discrepancy in flow angle observed. Figure 5 shows the entropy contour through the rotor blade. The largest fluid losses are present on the suction side of the blade, agreeing with the empirical model prediction.

C. Optimisation

Shape optimisation of the APU test case is studied here to demonstrate how the adjoint method can be used to improve the performance of a turbomachine (as well as how empirical models can be used to work alongside adjoint optimisation). The objective function to be minimized for this study is entropy generation, defined as

$$s_{gen} = \frac{T_{tot,in}}{v_{spout}^2} \sum_{k=1}^{3} (s_{out} - s_{in})_k$$

The optimisation is also constraint to the relative flow angle leaving the rotor $\beta_2 < 56°$. The design variables for this optimisation problem are defined using a free-form deformation box of degree six, i.e. six divisions along

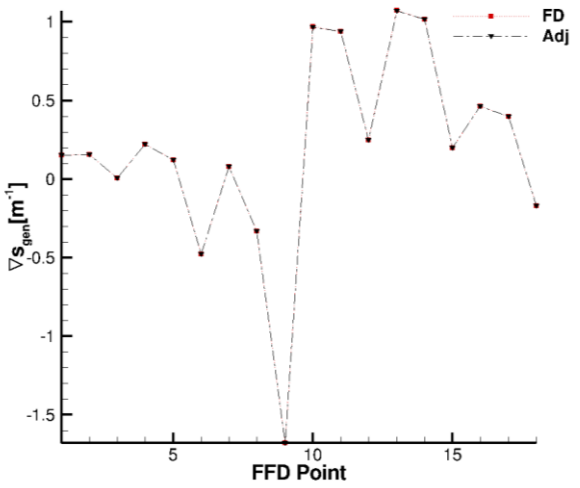

Figure 6 Comparison of entropy generation gradients calculated using a finite difference method and discrete adjoint method

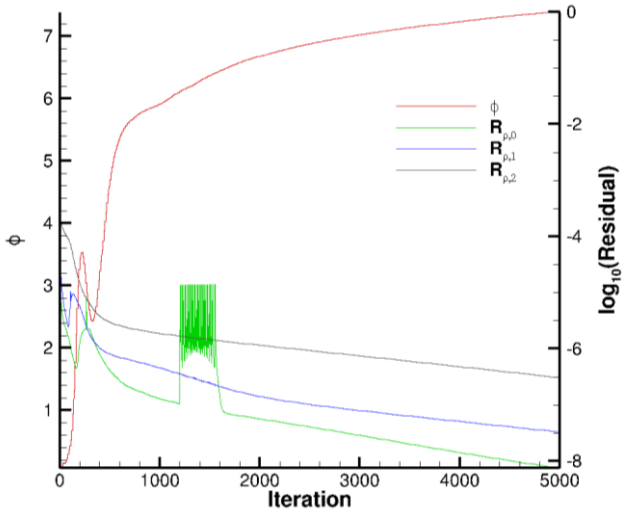

Figure 7 Convergence plot of the RANS adjoint solver

each of the hexahedron FFD box's box along each vertex, in each Cartesian direction around the rotor blade for a total number of 216 control points. The six ranks along each vertex compromising the FFD box intersect with the rotor blade for a total of 3904 intersection points. To ensure the mesh deformation algorithm does not produce unfeasible designs, the FFD box in the z-plane corresponding to the trailing edge was fixed. This resulted in 180 design variables. The preliminary optimisation study is conducted using a coarser mesh with a reduced cell count of 1 million elements and a first wall-normal spacing of $y^+ < 5.0$. The sequential lest squares programming (SQLSP) implemented in the Python toolbox SciPy is used as the optimisation algorithm.

Gradient Validation

Adding to the CFD validation detailed above, it is also necessary to perform a gradient validation to ensure that the gradients calculated via the adjoint method are accurate. To do this a finite difference algorithm is used to deform the mesh individually along the design variables, solve the flow field for each deformation, and then the resulting gradients for each design variable are calculated. These gradients are then compared to the adjoint gradient calculations. Due to the large computational cost required to solve the flow field for every design variable a reduced degree FFD box is used for the validation. An FFD box of degree one in each cartesian direction is chosen. The FFD box is again fixed in the final z-plane to prevent unfeasible trailing edge deformations. Additionally, the gradient calculation and resulting deformation is only performed in the x-radial direction. A nondimensional deformation step size of 1×10^{-5} was chosen for this study.

As shown in Figure 6 the gradients calculated due to adjoint method agree excellently with the gradients calculated using the finite differences routine. This demonstrates that the adjoint system detailed in Section III.D is being solved correctly.

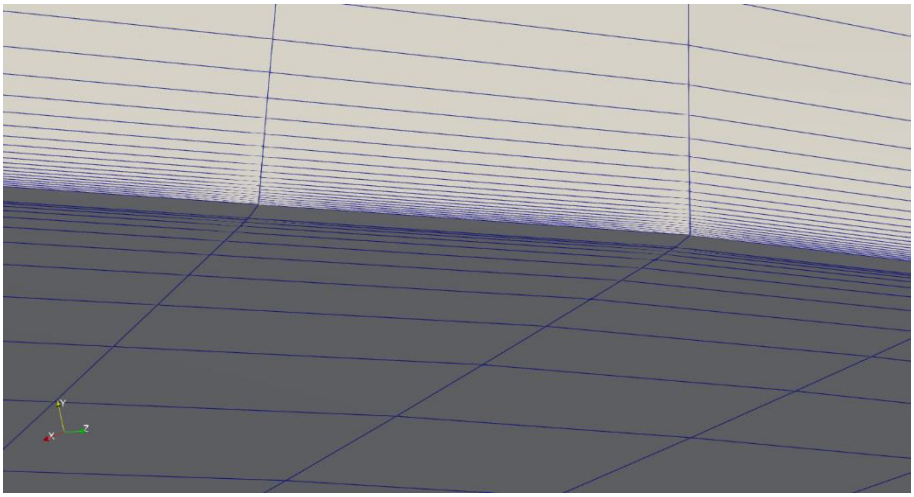

Figure 8 Distorted cells after deformation procedure between hub and blade near leading edge

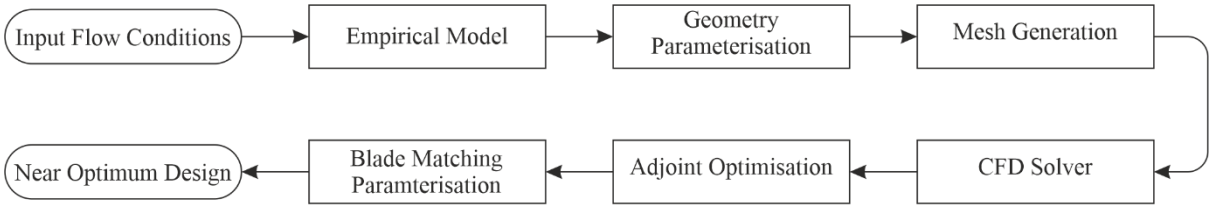

Figure 9 Flowchart of the proposed design framework

Geometry Optimisation

The adjoint solver setup requires further development to be successful. The plot in Figure 7 shows the convergence history for the adjoint solver as implemented using the method described previously. The geometry sensitivity is calculated as

$$\phi = \sum_{k=1}^{3} \left| \left| \bar{\boldsymbol{X}}_{k,blade} \right| \right|$$
$$with\ k = \{1,2,3\}$$

Within the turbine, the largest entropy generation gradients occur near the wall boundaries due to viscous drag. In this optimisation procedure the hub wall is not considered in the design variables. After the mesh deformation, cells at the boundary between the blade and the hub become significantly distorted, as shown in Figure 8. This results in the following CFD simulation to crash. To resolve this, future work can either consider the hub as a Euler wall in the flow solver boundary conditions, even though this would be less physical and would result in less accurate results, or consider the hub in the design variables and allow for simultaneous optimisation of hub and blade surfaces. Due to the nature of the adjoint formulation this will not affect the computational cost of the optimisation. Furthermore, the use of a mixing plane between the rotor and diffuser in this problem setup leads to the averaging out of significant entropy generating secondary flow structures that would be present in the diffuser if the flow were modelled to develop naturally.

V. Turboexpander Design Framework

The results in the previous sections demonstrate the steps required to complete the design of a radial inflow turboexpander. Using an empirical model, rapid initial geometry can be created. Through comparison to the APU test case, it is demonstrated that empirical methods produce excellent estimates for geometry and performance characteristics. Blade parameterisation and automated meshing tools can be used to generate quality geometry and grids based on the meridional channel geometries. High fidelity CFD is then used to solve the fluid domain modelled using RANS equations. Rotor motion is accounted for using the mixing-plane method with non-reflecting interface to produce a steady state solution. Coupling the CFD solver with an adjoint optimisation framework enables efficient, relatively fast calculation of optimum designs. The flowchart of the proposed design framework is shown in Figure 9. The steps detailed in this work enable the necessary steps for semi-automated design of future turboexpanders beyond current pressure limits. While for the test case described in this paper the adjoint solver and subsequent optimisation failed, the design framework is still feasible upon improvements to the

building blocks. Numerous authors have demonstrated that adjoint optimisation can be used for turbomachinery design[11–14,28]. The main advantage of this framework is the robustness of the adjoint optimisation method. If the flow solver can produce sufficiently accurate flow data, the method will eventually produce an optimum design. Also, the number of CFD simulations, and thus computational cost, is significantly reduced using this method. Deng et al.[35] developed a similar framework, using genetic algorithm, differential evolution, nondominated sorting genetic algorithm, and simulated annealing optimisation algorithms and applied it to the same test case detailed in this work. Their method required up to 1020 CFD simulations for the nozzle optimisation. This framework is capable of simultaneous multi blade row optimisation with a significantly reduced number of CFD simulations required. However, while the optimisation method is robust, the adjoint solver is less so and effort is still required to develop a model that will solve the adjoint equations accurately. For the design of future HPHT turboexpanders beyond the current pressure limit, there is a need for the understanding of the complex fluid flow present. This will require high-quality, large cell-count meshes which would be unsuitable for previous design methodologies. Additionally, while the focus of this work is a turboexpander design, the generic workflow presented in Figu could be applied for any turbomachinery case.

VI. Conclusion and Outlook

This work proposes a design framework for the design of future HPHT turboexpanders for energy recovery during natural gas extraction. The framework involves the generation of an initial geometry using empirical modelling, geometry parameterisation, automated mesh generation, CFD simulation and adjoint optimisation to create a near-optimum design. This approach allows for the integration of high-fidelity CFD-based optimisation in the early design phase of a turboexpander. In addition to the necessary modifications to the adjoint solver setup, some future improvements could be made to this framework. The empirical model could be expanded to include non-ideal equations of state, HPHT turboexpanders will operate in the supercritical fluid regime where the ideal gas relation assumed in this work will not be valid. SU2 is already capable of solving fluid flow problems in non-ideal conditions. The CFD solver could be extended to solve an unsteady problem, e.g. previous work has demonstrated the effectiveness of the harmonic balance method to overcome unsteady fluid dynamic design problems cost effectively[36]. The CFD model could also be improved by modelling the boundary between the rotor and diffuser as a matching interpolation, rather than a mixing plane. This modification prevents the averaging out of entropy generating secondary flow structures and will lead to better performance improvement than a mixing-plane approach. Finally, further study could couple the framework with a response surface model to prevent the optimisation procedure from tending towards a local optimum rather than a global optimum. The next step for this project is to apply this framework to the design of a HPHT turboexpander.

Acknowledgements

This work is jointly funded by Titan Electricity Ltd, the Manufacturing Technology Centre (MTC) and the Low Carbon Eco-Innovatory (LCEI). We thank the University of Liverpool for computing time on the high-performance computing system. The simulation data that support the findings of this study are available from the authors upon reasonable request. The first author thanks Dr M. Pini and Dr S. Vitale of TU Delft for their valuable discussions regarding SU2. This work was completed with the SU2 branch available at https://github.com/su2code/SU2/tree/feature_turbomachinery

References

1. UK Government. *UK hydrogen strategy*. https://www.gov.uk/government/publications/uk-hydrogen-strategy (2021).
3. Bauer, C. *et al.* On the climate impacts of blue hydrogen production. *Sustainable Energy and Fuels* **6**, (2022).
4. Howarth, R. W. & Jacobson, M. Z. How green is blue hydrogen? *Energy Science and Engineering* **9**, (2021).
5. Atlas Copco. Driving expander technology. https://www.atlascopco.com/content/dam/atlas-copco/compressor-technique/gas-and-process/documents/5626-Driving-expander-technology-LR.pdf.
6. Li, Z. & Zheng, X. Review of design optimization methods for turbomachinery aerodynamics. *Progress in Aerospace Sciences* vol. 93 Preprint at https://doi.org/10.1016/j.paerosci.2017.05.003 (2017).
7. Peter, J. E. V. & Dwight, R. P. Numerical sensitivity analysis for aerodynamic optimization: A survey of approaches. *Computers and Fluids* vol. 39 Preprint at https://doi.org/10.1016/j.compfluid.2009.09.013 (2010).
8. Pironneau, O. On optimum design in fluid mechanics. *Journal of Fluid Mechanics* **64**, (1974).
9. Jameson, A. Aerodynamic design via control theory. *Journal of Scientific Computing* **3**, (1988).

10. Jameson, A. Optimum aerodynamic design using CFD and control theory. in *12th Computational Fluid Dynamics Conference* (1995). doi:10.2514/6.1995-1729.
11. Li, Y., Yang, D. & Feng, Z. Inverse problem in aerodynamic shape design of turbomachinery blades. in *Proceedings of the ASME Turbo Expo* vol. 6 PART B (2006).
12. Arens, K., Rentrop, P., Stoll, S. O. & Wever, U. An adjoint approach to optimal design of turbine blades. in *Applied Numerical Mathematics* vol. 53 (2005).
13. Wu, H. Y., Liu, F. & Tsai, H. M. Aerodynamic design of turbine blades using an adjoint equation method. in *43rd AIAA Aerospace Sciences Meeting and Exhibit - Meeting Papers* (2005). doi:10.2514/6.2005-1006.
14. Walther, B. & Nadarajah, S. Optimum shape design for multirow turbomachinery configurations using a discrete adjoint approach and an efficient radial basis function deformation scheme for complex multiblock grids. *Journal of Turbomachinery* **137**, (2015).
15. Aungier, R. H. *Turbine Aerodynamics: Axial-Flow and Radial-Flow Turbine Design and Analysis*. *Turbine Aerodynamics: Axial-Flow and Radial-Flow Turbine Design and Analysis* (2010). doi:10.1115/1.802418.
16. Rohlik, H. Analytical determination of radial inflow turbine design geometry for maximum efficiency. *NASA TN D-4384.1969.* (1969).
17. Glassman, A. J. Computer program for design analysis of radial-inflow turbines. *NASA Technical Note* (1976).
18. Glassman, A. J. *Turbine Design And Application*. *Nasa* (1994).
19. Menter, F. R. Two-equation eddy-viscosity turbulence models for engineering applications. *AIAA Journal* **32**, (1994).
20. Menter, F. R. AIAA 93 · 2906 Zonal Two Equation k-w Turbulence Models for Aerodynamic Flows. in *American Institute of Aeronautics and Astronautics: 24th Fluid Dynamics Conference* (1993).
21. Versteeg, H. K. *et al. An Introduction to Computational Fluid Dynamics - The Finite Volume Method*. *Fluid flow handbook. McGraw-Hill …* (1995).
22. Economon, T. D., Palacios, F., Copeland, S. R., Lukaczyk, T. W. & Alonso, J. J. SU2: An open-source suite for multiphysics simulation and design. *AIAA Journal* **54**, (2016).
23. Roe, P. L. Approximate Riemann solvers, parameter vectors, and difference schemes. *Journal of Computational Physics* vol. 43 Preprint at https://doi.org/10.1016/0021-9991(81)90128-5 (1981).
24. Saad, Y. A Flexible Inner-Outer Preconditioned GMRES Algorithm. *SIAM Journal on Scientific Computing* **14**, (1993).
25. Albring, T., Sagebaum, M. & Gauger, N. R. Efficient aerodynamic design using the discrete adjoint method in SU2. in *17th AIAA/ISSMO Multidisciplinary Analysis and Optimization Conference* (2016). doi:10.2514/6.2016-3518.
26. Denton, J. D. The calculation of three-dimensional viscous flow through multistage turbomachines. *Journal of Turbomachinery* **114**, (1992).
27. Saxer, A. P. & Giles, M. B. Predictions of three-dimensional steady and unsteady inviscid transonic stator/rotor interaction with inlet radial temperature nonuniformity. *J of Turbomachinery* **116**, (1994).
28. Vitale, S., Pini, M. & Colonna, P. Multistage turbomachinery design using the discrete adjoint method within the open-source software su2. *Journal of Propulsion and Power* **36**, (2020).
29. Albring, T., Sagebaum, M. & Gauger, N. R. Efficient aerodynamic design using the discrete adjoint method in SU2. in *17th AIAA/ISSMO Multidisciplinary Analysis and Optimization Conference* (2016). doi:10.2514/6.2016-3518.
30. Dwight, R. P. Robust mesh deformation using the linear elasticity equations. in *Computational Fluid Dynamics 2006 - Proceedings of the Fourth International Conference on Computational Fluid Dynamics, ICCFD 2006* (2009). doi:10.1007/978-3-540-92779-2_62.
31. Sederberg, T. W. & Parry, S. R. Free-form deformation of solid geometric models. in *Proceedings of the 13th Annual Conference on Computer Graphics and Interactive Techniques, SIGGRAPH 1986* (1986). doi:10.1145/15922.15903.
32. Jones, A. C. Design and test of a small, high pressure ratio radial turbine.*J of Turbomachinery* **118**, (1996).
33. Sauret, E. Open design of high pressure ratio radial-inflow turbine for academic validation. in *ASME International Mechanical Engineering Congress and Exposition, Proceedings (IMECE)* vol. 7 (2012).
34. Agromayor, R., Anand, N., Müller, J. D., Pini, M. & Nord, L. O. A Unified Geometry Parametrization Method for Turbomachinery Blades. *CAD Computer Aided Design* **133**, (2021).
35. Deng, Q., Shao, S., Fu, L., Luan, H. & Feng, Z. An integrated design and optimization approach for radial inflow turbines-part II: Multidisciplinary optimization design. *Applied Sciences (Switzerland)* **8**, (2018).
36. Rubino, A., Vitale, S., Colonna, P. & Pini, M. Fully-turbulent adjoint method for the unsteady shape optimization of multi-row turbomachinery. *Aerospace Science and Technology* **106**, (2020).